Debris flow susceptibility mapping in Colorado Front Range, USA: a comparison of physics-based and data-driven approaches

Te Pei[1], and *Tong* Qiu[1*]

[1]Department of Civil and Environmental Engineering, The Pennsylvania State University, University Park, PA 16802, USA

Abstract. This study used an inventory of debris flow triggered by a storm event in Colorado Front Range as an example to compare the capability of data-driven and physics-based approaches for regional-scale debris flow susceptibility mapping (LSM). Nine debris flow contributing factors were collected for the present study based on the availability of geophysical data in the study area. These contributing factors represent hillslope geometries, surface hydrology, and soil conditions. For the physics-based approach, the infinite slope model was used to directly determine the debris flow susceptibility for the study area by calculating the factor of safety (FS) based on parameters derived from geophysical data. For the data-driven approach, an artificial neural network (ANN) was developed to predict debris flow susceptibility for the study area by learning relationships from the contributing factors using the debris flow inventory. The results showed that both physics-based and data-driven models predicted debris flow susceptibility in the study area with relatively high accuracy; the data-driven approach outperformed the physics-based approach as it could extract complex features which the physics-based approach did not consider.

1 Introduction

Debris flows are common natural disasters around the globe. Understanding where these landslide hazards are likely to occur is essential for hazard mitigation and provides situational awareness for the public.

Landslide susceptibility mapping (LSM) measures the spatial distribution of landslide risk given a combination of contributing factors [1]. Methods for LSM can be broadly classified into physics-based and data-driven methods. The physics-based methods rely on the physics understanding of slope failure in soil mechanics. For example, the infinite slope model has been widely used to evaluate landslide risk for rainfall-induced shallow landslides on natural terrain (e.g., [2-4]). However, accurate input parameters for physics-based approaches, such as soil strength and hydrological parameters, are relatively difficult to obtain on a regional scale. In addition, the performance of physics-based approaches may be limited due to simplified physical assumptions. On the other hand, data-driven approaches establish functional relationships between landslide risk and contributing factors based on observations of landslide occurrence (e.g., [5-8]). The research community has been currently focusing on data-driven methods due to the recent advances in remote sensing and machine learning (ML) techniques [9].

In the present study, LSM was conducted for a debris flow-affected region in Colorado Front Range using both physics-based and data-driven approaches. The debris flow inventory and study area are first described in the following sections, followed by descriptions of the debris flow contributing factors and methodologies. Last, the performance of developed LSM models using the two approaches was evaluated and compared, and debris flow susceptibility maps for the study area were produced.

2 Study area and debris flow inventory

The Colorado Front Range is a mountain range of the Southern Rocky Mountains of North America located in the central portion of the State of Colorado. It is formed by orogenic uplift related to regional compression during the Laramide orogeny in the Late Cretaceous to early Tertiary [10]. The Colorado Front Range has a broad elevation variation ranging between 1,500 m and 4,300 m; it spans four major topographic elements and five ecosystem zones [11, 12]. The vegetation density, soil development, and regolith production are dependent on the slope aspect [13]. Boulder County in the Colorado Front Range area was selected as the study area, where 60% of the mapped debris flows were located in this County.

The present study used a well-documented debris flow inventory to develop and evaluate the performance of LSM models. A storm event in September 2013 triggered more than one thousand debrie flows across the Colorado Front Range. Detailed information for

* Corresponding author: tuq1@psu.edu

these debris flows was recorded based on a reconnaissance through field survey and high-resolution orthorectified satellite imagery following the storm event. Specifically, 1,138 debris flows and 212 slides were identified and mapped [12]. Fig. 1 presents the location of Boulder County and the distribution of mapped debris flow locations.

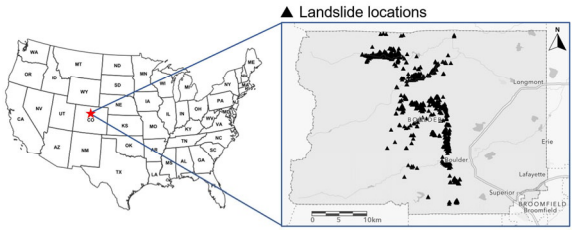

Fig. 1. Location of Boulder County and distribution of debris flow events triggered by the 2013 storm event.

3 Collection of geophysical data

In the present study, nine debris flow contributing factors were chosen based on the data availability and types of debris flow that occurred in the study area, including elevation, slope, aspect, topographic wetness index (TWI), normalized difference vegetation index (NDVI), sand content, clay content, bulk density, and field capacity. These contributing factors reflect the effects of hillslope geometries, hydrologic conditions, and soil properties. Fig. 2 shows a contour plot of these contributing factors in the study area.

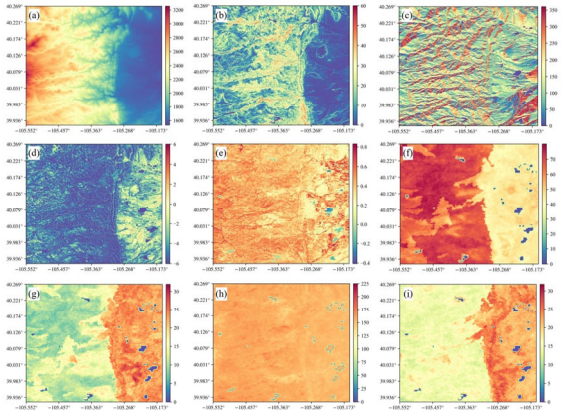

Fig. 2. Debris flow contributing factors for the study area: (a) elevation (m); (b) slope (deg); (c) aspect (deg); (d) TWI (-); (e) NDVI (-); (f) sand content (%); (g) clay content (%); (h) bulk density (10 kg/m^3); and (i) field capacity (%).

Among these contributing factors, the elevation is based on the digital elevation model (DEM) provided by the 3D Elevation Program (3DEP) with 10-m spatial resolution. The slope and aspect were calculated from the DEM, representing the slope geometries and facing directions. The TWI was also calculated from the DEM to represent topographic control on surface hydrology. The NDVI was calculated based on near-infrared and red bands from Landsat-8 satellite images and was used to represent vegetation coverage. The soil information was obtained from SoilGrids [14], which provides a global estimation of surface soil properties based on soil profiles and remote sensing data with a spatial resolution of 250 m. Fig. 2 shows a contour plot of these contributing factors in the study area.

4 Methodologies

The development of LSM models for the present study involves several key steps, including dataset preparation, LSM model development and evaluation, and generation of final landslide susceptibility map. Fig. 3 illustrates the workflow for the present study.

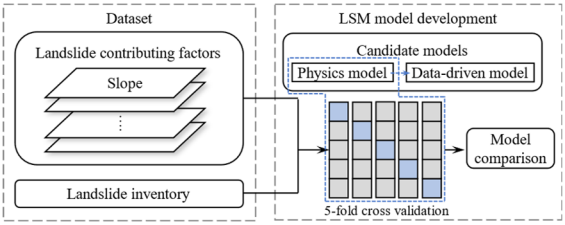

Fig. 3. Workflow for the present study.

4.1 Dataset preparation

For the present study, 803 mapped debris flow locations in the study area and their corresponded values of debris flow contributing factors were used as positive samples. An equal amount of non-debris flow locations were randomly sampled within the study area, excluding those debris flow locations. These non-debris flow points and their corresponding values of contributing factors were used as negative samples.

4.2 Physics-based model

The infinite slope model was selected as the physics-based model for the present study, which is commonly used for predicting shallow landslides such as the debris flows in this study. The factor of safety (FS) is calculated as the ratio between the soil shear strength and the driving force:

$$FS = \frac{c + (\gamma H - \gamma_w h)\cos^2\beta \tan\phi}{\gamma H \sin\beta \cos\beta} \quad (1)$$

where h is the height of the groundwater table; H is the soil layer thickness; γ is the soil unit weight; γ_w is the unit weight of water; β is the slope angle; and ϕ and c are the soil friction angle and cohesion, respectively. For simplicity, submerged slopes with seepage parallel to the slope were assumed when calculating FS (i.e., $h = H$). The input parameters for the infinite slope model were estimated based on the debris flow contributing factors. For example, β is based on the slope from DEM. H is estimated based on an elevation-dependent relationship as [15]:

$$H = H_{max} - \frac{Z - Z_{min}}{Z_{max} - Z_{min}}(H_{max} - H_{min}) \quad (2)$$

where H and Z are the local soil layer thickness and elevation, respectively; H_{min} and Z_{min} are the minimum soil layer thickness and elevation, respectively; H_{max} and Z_{max} are the maximum soil layer thickness and elevation, respectively. For the present study, $H_{min} = 5$ cm and $H_{max} = 2$ m. ϕ is estimated using sand content and an empirical relationship from [16]. For estimating c, the soil itself is cohesionless [17]; however, root reinforcement in slope stability was considered. The values of c were obtained by applying a linear transformation to the full spectrum values of NDVI [18] by setting the minimum cohesion of value 0.0 kPa and the maximum at 15.0 kPa.

4.3 Data-driven model

From the data science perspective, the application of LSM can be considered a classification problem where features of debris flow contributing factors are extracted and grouped based on their relationships and contributions to the debris flow label. For the present study, an artificial neural network (ANN) with three hidden layers was used to represent a data-driven model, which is a commonly used model in ML.

4.4 Performance evaluations

The present study used the 5-fold cross-validation technique [19] for model performance evaluation, corresponding to an 80%/20% sample split. In cross-validation, the dataset is divided into five folds, and the model is trained using four folds and validated using the remaining one fold. This process repeats five times to allow each fold to be served as a validation fold, and the final model performance is the average model performance for each validation fold.

The performance of classification models is typically evaluated based on the confusion matrix and receiver operating characteristic (ROC) curve. The ROC curve is a 2D plot of false positive rate (FPR) vs. true positive rate (TPR) for all classification thresholds. The FPR and TPR can be calculated as:

$$TPR = \frac{TP}{TP + FN} \quad (3)$$

$$FPR = \frac{FP}{FP + TN} \quad (4)$$

The area under the ROC curve (AUC) can be calculated based on the ROC curve, which is often used as a single-value evaluation for classification models. It measures the model's capability to distinguish two classes. The AUC score was used as the performance indicator for the present study.

5 Results and discussion

Table 1 presents the AUC scores for the infinite slope and the ANN models based on the same five-fold cross-validation procedure. Typically, a classification model with AUC scores greater than 0.9 can be considered an excellent classifier. As shown in Table 1, both the infinite slope model and the ANN model achieved relatively high AUC scores, indicating that the two approaches can be successfully applied to predict the debris flow susceptibility in the study area. In addition, the ANN model yielded a higher AUC score than the infinite slope model, which can be attributed to the fact that the ANN model was able to directly extract complex features from data based on debris flow labels, including those hidden features the physics-based model fails to consider.

Table 1. Cross-validation results for LSM models

Models	Avg. AUC
Infinite slope model	0.894
ANN model	0.930

Furthermore, the developed LSM models based on the two approaches were subsequently used to predict debris flow risk for the study area. Figs. 4 and 5 present the debris flow susceptibility maps using the two approaches, where mapped debris flow locations are shown as black triangles. By comparing Figs. 4 and 5, it can be noted that the high debris flow risk areas predicted by both approaches generally agreed well with the mapped debris flow locations, and the areas with high susceptibility but were not mapped by the reconnaissance following the 2013 event can be considered debris flow-prone areas. In addition, it can be noted that the ANN model tends to over-estimate debris flow risks compared to the infinite slope model, especially in the west part of the study area, which can also attribute to the hidden features extracted by the ANN model. Additional study is recommended to investigate the generalization capabilities of data-driven models on LSM.

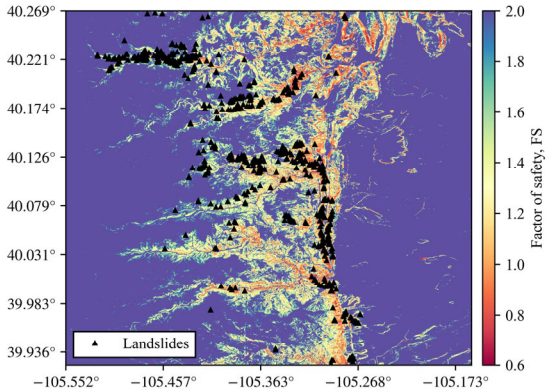

Fig. 4. Debris flow susceptibility map for the study area based on the infinite slope model.

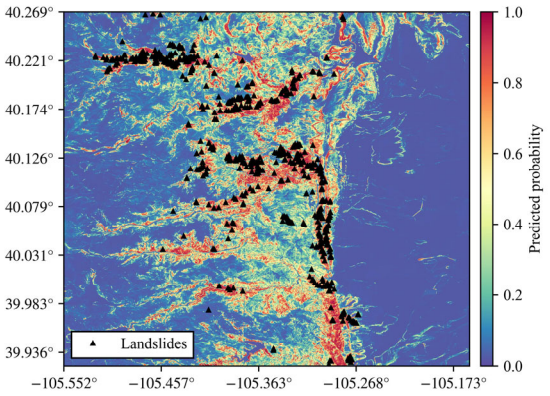

Fig. 5. Debris flow susceptibility map for the study area based on the ANN model.

6 Conclusion

Through a case study on debris flows triggered by a storm event in Colorado Front Range, this study compares the capabilities of physics-based and data-driven approaches for LSM on a regional scale. Based on the cross-validation results, both approaches can be successfully used to predict debris flow risks across the study area with appropriately selected debris flow contributing factors, and the data-driven approach was able to outperform the physics-based approach in terms of the AUC score. However, it should be noted that the successful application of data-driven approaches requires high-quality debris flow inventory with a sufficient amount of debris flow records, which may not be available in certain applications. On the other hand, using domain knowledge, physics-based approaches can provide debris flow risk estimates in a label-free fashion.

This research was partially supported by Google AI Impact Challenge Grant 1904-57775. The second author's effort was supported by the U.S. National Science Foundation under Award No. ICER-2022444. These supports are gratefully acknowledged.

References

1. F. Guzzetti, P. Reichenbach, M. Cardinali, M. Galli, and F. Ardizzone, Geomorphology (Amst), **72** (1–4), 272–299 (2005)
2. L. Montrasio and R. Valentino, Nat. Hazards Earth Syst. Sci., **8** (5), 1149–1159 (2008)
3. R. L. Baum, J. W. Godt, and W. Z. Savage, J. Geophys. Res., **115** (F3) (2010)
4. X. He, Y. Hong, H. Vergara, K. Zhang, P.-E. Kirstetter, J. J. Gourley, Y. Zhang, G. Qiao, and C. Liu, J. Hydrol., **543**, 395–405 (2016)
5. P. Tsangaratos, I. Ilia, Landslides, **13** (2), 305–320 (2016)
6. S. Lee, S.-M. Hong, and H.-S. Jung, Sustainability, **9** (1): 48 (2017)
7. L. Xiao, Y. Zhang, and G. Peng, Sensors, **18** (12), 4436 (2018)
8. Y. Wang, Z. Fang, and H. Hong, Sci. Total Environ., **666**, 975–993 (2019)
9. P. Reichenbach, M. Rossi, B. D. Malamud, M. Mihir, and F. Guzzetti, Earth Sci. Rev., **180**, 60–91 (2018)
10. W. R. Dickinson, M. A. Klute, M. J. Hayes, S. U. Janecke, E. R. Lundin, M. A. McKittrick, and M. D. Olivares. Geol. Soc. Am. Bull., 100 (7), 1023–1039 (1988)
11. R. S. Anderson, C. A. Riihimaki, E. B. Safran, and K. R. MacGregor. *in Tectonics, Climate and Landscape Evolution*, edited by S. D. Willett et al., Spec. Pap. Geol. Soc. Am., **398**, 397 – 418 (2006)
12. J. A. Coe, J. W. Kean, J. W. Godt, R. L. Baum, E. S. Jones, D. J. Gochis, and G. S. Anderson, GSA Today, **24** (10), 4–10 (2014)
13. P. W. Birkeland, R. R. Shroba, S. F. Burns, A. B. Price, and P. J. Tonkin, Geomorphology, **55** (1–4), 329–344 (2003)
14. T. Hengl, J. Mendes de Jesus, G. B. M. Heuvelink, M. Ruiperez Gonzalez, M. Kilibarda, A. Blagotić, W. Shangguan, M. N. Wright, X. Geng, B. Bauer-Marschallinger, M. A. Guevara, R. Vargas, R. A. MacMillan, N. H. Batjes, J. G. B. Leenaars, E. Ribeiro, I. Wheeler, S. Mantel, and B. Kempen, PLoS One, **12** (2): e0169748 (2017)
15. G.-M. Saulnier, K. Beven, and C. Obled, J. Hydrol., **202**, 158–172, (1997)
16. J. Park, and J. C. Santamarina, J. Geotech. Geoenviron. Eng., **143** (8), 04017039 (2017)
17. L. Southerland, W. Zhou, Environ. Eng. Geosci., **27** (4), 471–486 (2021)
18. J.-C. Huang, S.-J. Kao, M.-L. Hsu, and J.-C. Lin, Nat. Hazards Earth Syst. Sci., **6** (5): 803–815 (2006)
19. M. Stone, J. R. Stat. Soc., **36** (2), 111–133 (1974)